

# Dalton Transactions

Accepted Manuscript



This is an *Accepted Manuscript*, which has been through the Royal Society of Chemistry peer review process and has been accepted for publication.

*Accepted Manuscripts* are published online shortly after acceptance, before technical editing, formatting and proof reading. Using this free service, authors can make their results available to the community, in citable form, before we publish the edited article. We will replace this *Accepted Manuscript* with the edited and formatted *Advance Article* as soon as it is available.

You can find more information about *Accepted Manuscripts* in the [Information for Authors](#).

Please note that technical editing may introduce minor changes to the text and/or graphics, which may alter content. The journal's standard [Terms & Conditions](#) and the [Ethical guidelines](#) still apply. In no event shall the Royal Society of Chemistry be held responsible for any errors or omissions in this *Accepted Manuscript* or any consequences arising from the use of any information it contains.

# Structural and Bonding Patterns in Gold Clusters<sup>1</sup>

D. Michael P. Mingos\*

\**Inorganic Chemistry laboratory, Oxford University, South Parks Road, Oxford OX1 3QR, UK. Email: michael.mingos@seh.ox.ac.uk*

**Received:**

**Accepted:**

---

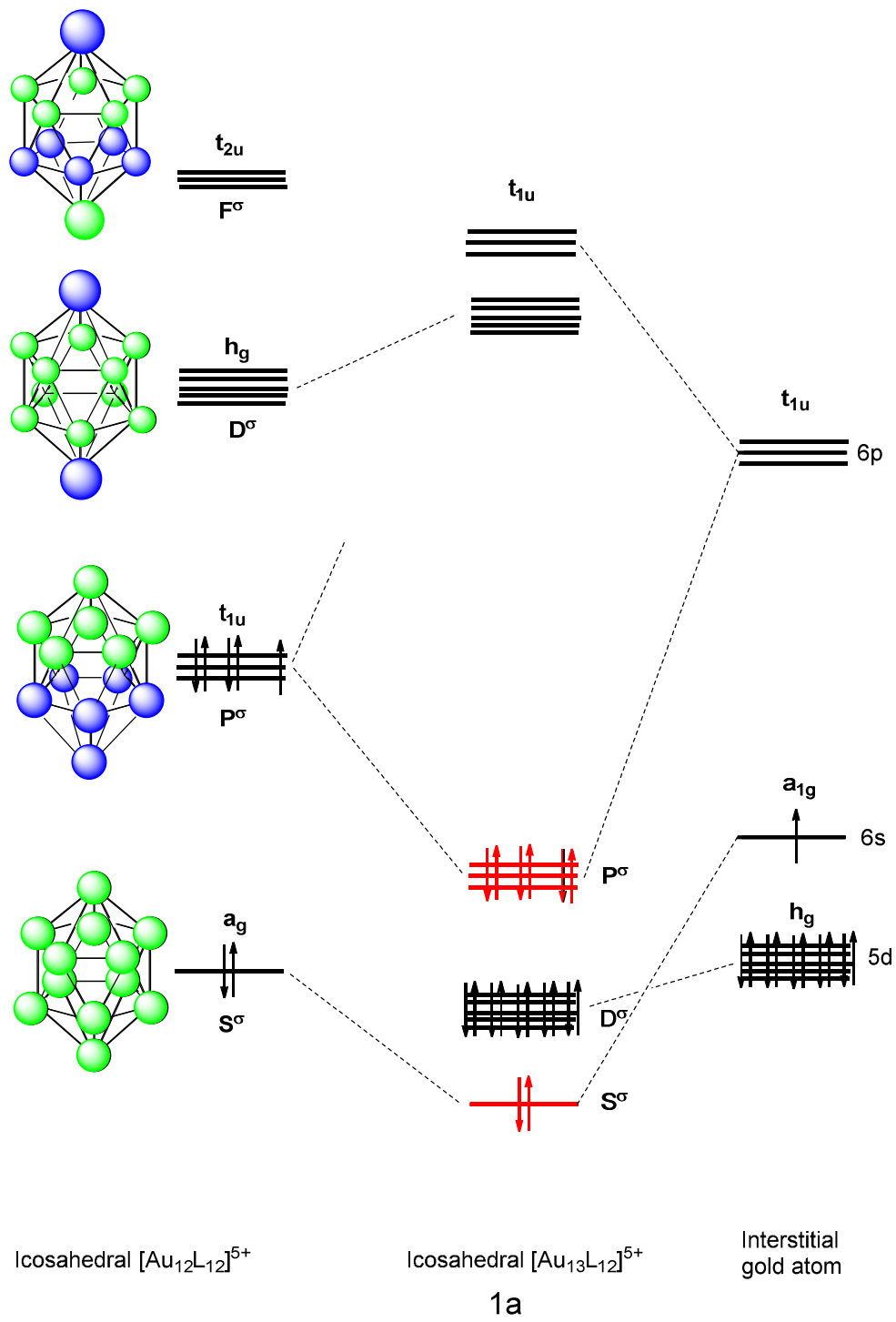
The study of gold cluster compounds originated from Malatesta's syntheses of tertiaryphosphine derivatives in the 1960s and was greatly extended between 1970 and 2000. Single crystal X-ray studies defined the major structural classes and led to the development of a theoretical model which accounted for their closed shell requirements in terms of their topological features and proved to be sufficiently flexible to be extended to related heteronuclear cluster compounds. Since the turn of the century the range of gold cluster compounds has been greatly extended by the study of organothiolato- gold cluster compounds. The structures of these compounds have revealed that the gold atoms combine with the organothiolato- ligands to generate a novel class of metallo-organothiolato-ligands which protect and stabilise the inner core of gold atoms. These developments originally suggested that the phosphine and organothiolato- clusters defined quite distinct classes of gold clusters, but recent structural and theoretical developments have reconciled many of these differences. This review summarises the structures of all the clusters of gold and suggests a theoretical model which effectively unites the broad structural properties of the two classes of compound. This model is based on the united atom model for diatomics developed by Mulliken and the compression co-ordinate is related to the interpenetration of icosahedral and cuboctahedral pseudo- spherical clusters. The predicted closed shell requirements agree well with the results of structural determinations.

## Introduction

Following the initial flurry of publications in 1971-1975 introducing the *Polyhedral Skeletal Electron Pair Theory* (PSEPT)<sup>1-5</sup> I shifted my attention to understanding the fundamental electronic basis of the rules and the reasons for the analogy between main group and transition metal carbonyl clusters. This led to a definition of the capping principle<sup>6</sup> and the *isolobal* analogy<sup>7</sup> and a molecular orbital analysis which emphasised the commonality of the antibonding skeletal molecular orbitals in  $[\text{B}_6\text{H}_6]^{2-}$  and  $[\text{Co}_6(\text{CO})_{14}]^{4-}$ .<sup>8</sup> This analysis demonstrated that the number and symmetries of the unavailable molecular orbitals in polyhedral molecules was crucial in defining the relationship between borane and transition metal carbonyl clusters. I also studied many classes of molecules which did not conform to the electron counting rules.<sup>9-13</sup> Ken Wade in his major review published in 1976<sup>14</sup> made the

---

<sup>1</sup> This review is based on the lecture given by DMPM at the Ken Wade Commemoration Symposium at Durham University on Monday 15<sup>th</sup> December 2014. Although DMPM and Ken Wade never published together their names are usually linked to the development of the nexus of structural patterns and bonding ideas which have underpinned cluster chemistry since the 1970s.



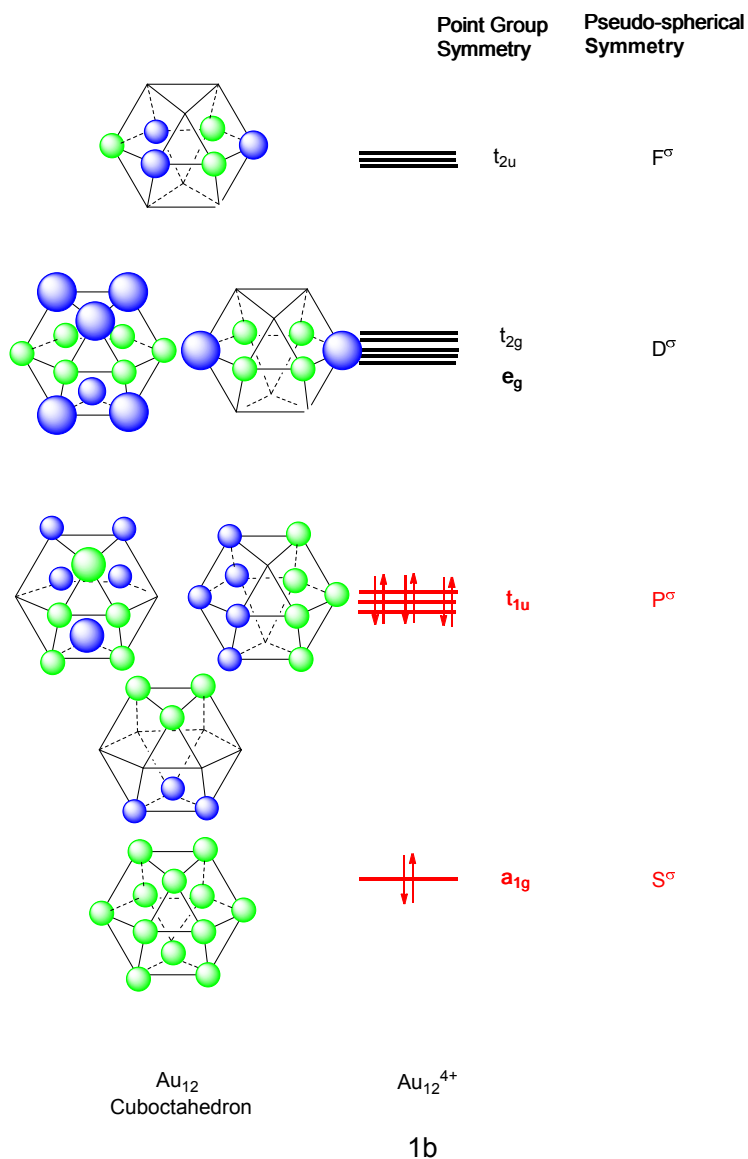


**Figure 1a.** Illustration of the skeletal molecular orbitals in a centred icosahedral gold cluster. The molecular orbitals are labelled using the point group symmetries of the  $I_h$  point group and the pseudo-spherical symmetry labels  $S^\sigma$ ,  $P^\sigma$ ,  $D^\sigma$ ,  $F^\sigma$ . **Figure 1b.** Skeletal molecular orbitals of a cuboctahedral gold cluster shown as LCAOs of the gold 6s orbitals. The reduced number of nearest gold-gold interactions destabilises this geometry relative to the icosahedron. The 8 electrons which constitute the **sec** of 8 are shown in red. The **sec** is equal to the total number of gold 6s valence electrons.

following comment on gold-phosphine clusters “A simple convincing bonding rationale for their structures has yet to be found”. I submitted to Dalton Transactions a description of the bonding in these clusters at the end of 1975 and suggested that gold clusters differed from metal-carbonyls, because their tangential  $\pi$ -orbitals are not sufficiently stable to contribute to skeletal bonding, i.e. they are unavailable for metal-metal bonding.<sup>15</sup> The metal-metal bonding is dominated by radial and tangential interactions based on the s and  $d_{z^2}$  orbitals of the gold atoms. A simple spectrum of skeletal molecular orbitals results, which resembles

those found in alkali metal clusters. Specifically, the occupation of these molecular orbitals in spherical gold clusters leads to closed shells analogous to those found in atoms and familiar to chemists, i.e.  $[S^\sigma]^2$ ;  $[S^\sigma]^2[P^\sigma]^6$ ;  $[S^\sigma]^2[P^\sigma]^6[D^\sigma]^{10}$ ; etc..<sup>15-19</sup> Schematic illustrations of the skeletal MOs for a spherical icosahedral centred and cuboctahedral gold clusters are shown in Figure 1.

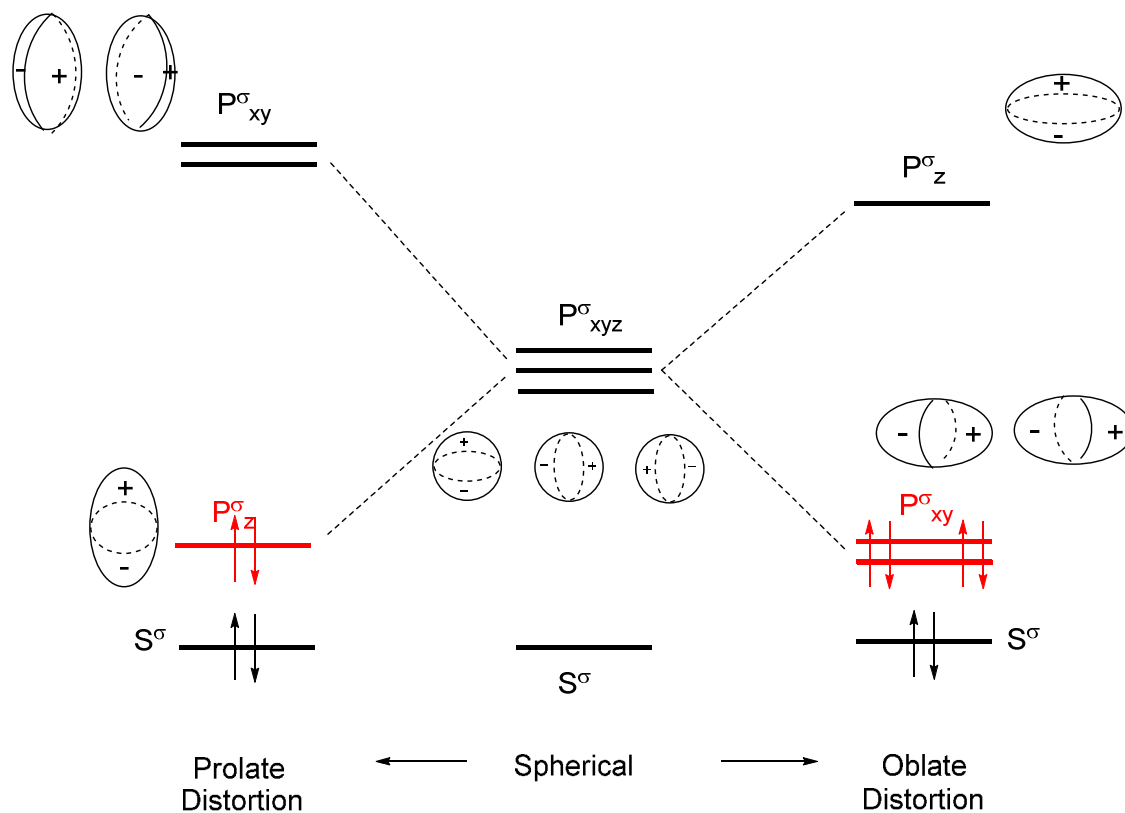


**Figure 2** . Removal of the degeneracy of the  $P^\sigma$  shell in non-spherical gold clusters

Gold clusters with non-spherical geometries cause the removal of the degeneracy of the  $P^\sigma$  shell as shown in Figure 2. If the asymmetry induced by prolate or oblate distortions is substantial, the energy gap which results is sufficiently large for the stabilisation of closed sub-shell electronic structures, i.e.  $[S^\sigma]^2[P^\sigma]^2$  for prolate and  $[S^\sigma]^2[P^\sigma]^4$  for oblate. *Aufbau* filling of the skeletal molecular orbitals shown in Figure 2 results in the following series of diamagnetic gold clusters 2e (spherical); 4e (prolate); 6e (oblate) and 8e (spherical).<sup>15-19</sup> The translation of spherical, prolate and oblate designations into specific polyhedral shapes is assisted by choosing those which maximise the number of near-neighbour Au-Au interactions, i.e. deltahedral geometries are favoured. The structurally characterised clusters illustrated in Figure 3 verify the value of this simple analysis. This pattern is reproduced in part for gold clusters with interstitial main group or transition metal atoms, i.e. 6e (oblate or toroidal) and 8e (spherical). An extensive series of clusters with interstitial gold (and platinum) atoms have been structurally characterised and some of the relevant examples are

illustrated in Figure 4.<sup>17-18</sup> It is noteworthy that the structures shown in this Figure are based on a centred chair of gold atoms. Spherical structures result by the addition of gold atoms along the three fold symmetry axis, whereas oblate structures result from edge bridging the chair. A similar series has been observed for a centred crown of gold atoms. It is noteworthy that this simple model based on semi-empirical calculations and reported in the 1976 paper predicted specific icosahedral and octahedral clusters, which were subsequently synthesised and structurally characterised in the 1980s.<sup>20-25</sup>

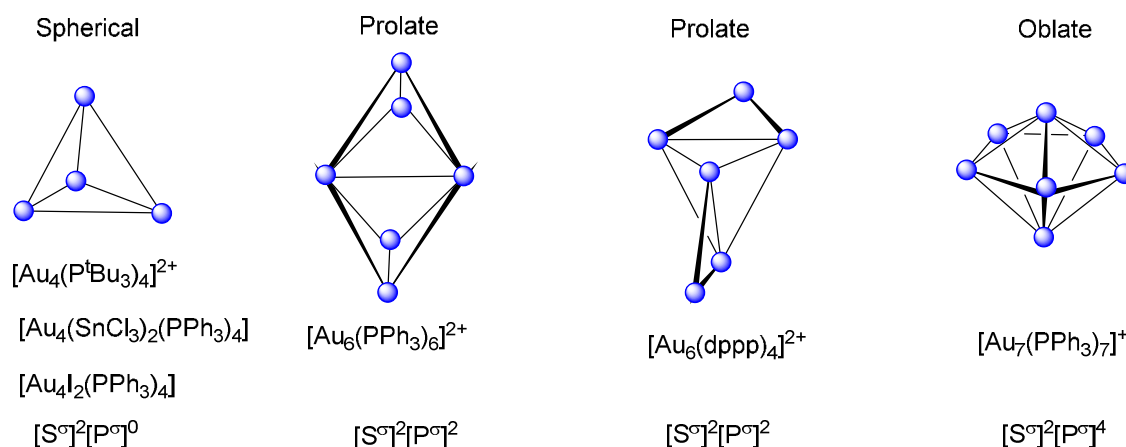


**Figure 3.** Examples of spherical -  $[\text{S}^\sigma]^2$ ; prolate -  $[\text{S}^\sigma]^2[\text{P}^\sigma]^2$  and oblate -  $[\text{S}^\sigma]^2[\text{P}^\sigma]^4$  clusters of gold. Dppp is  $\{\text{PPh}_2\}_2\text{C}_3\text{H}_6$ .

Gold clusters stabilised by thiolato- ligands rather than phosphines have attracted considerable interest recently because of their potential applications in the area of nanotechnology.<sup>26-28</sup> The rapid growth of the area has been stimulated by the development of a flexible general synthetic route which has led to the isolation of a number of crystalline materials and single crystal X-ray diffraction studies on some key compounds. The crystallographic determinations of  $[\text{Au}_{102}(\text{SC}_6\text{H}_4\text{CO}_2\text{H})_{44}]$  and  $[\text{Au}_{25}(\text{SC}_2\text{H}_4\text{Ph})_{18}]^-$  proved to be pivotal in developing an understanding of the important structural features.<sup>29,30</sup> Specifically they established that there is a central core of gold atoms, which is approximately spherical and close packed, and is stabilised by an outer layer of either SR or organothiolato-gold(I) ligands, e.g.  $\text{SR}^-$ ,  $[\text{Au}(\text{SR})_2]^-$  and  $[\text{Au}_2(\text{SR})_3]^-$ . These gold-thiolato-ligands have been described as “staples”, because they are considered to be essential for stabilising the gold core.<sup>31-37</sup>

The commonly observed “staples” are illustrated in Figure 5. From a co-ordination chemist’s point of view “staples” may be classified as bidentate metallo-thiolato- ligands capable of donating 4 electrons. The “staple ligands” have different bite angles according to the number of metal atoms and this enables them to span different sections of the central core and differentiate convex and concave parts of the core as shown in Figure 6. Initially, the occurrence of gold atoms in the central cluster core and as part of the “staples” represented a barrier for the application of the *Polyhedral Skeletal Electron Pair Theory*, which had been developed for clusters where there was a clear distinction between ligand shell and the metal core. In such clusters the polyhedral skeletal electron count is the sum of the electrons

donated by the ligands and the number of valence electrons in the metal core. As Häkkinen pointed out<sup>31-37</sup>:  $\text{SR}^-$ ,  $[\text{Au}(\text{SR})_2]^-$  and  $[\text{Au}_2(\text{SR})_3]^-$  are all 4 electron donors and bear a single

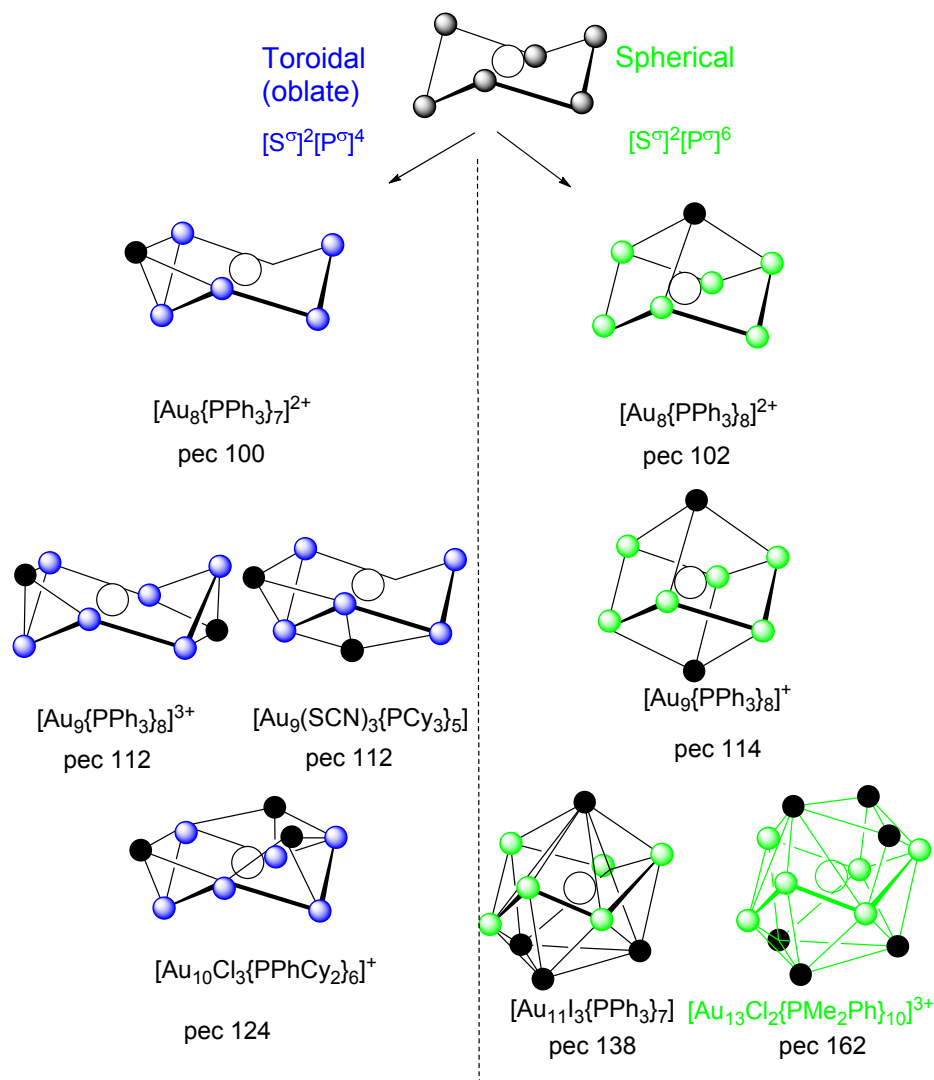


**Figure 4.** Examples of oblate and spherical gold phosphine clusters which contain an interstitial gold atom. The atoms in black represent additions to the basic centred crown arrangement of gold atoms. The spherical gold clusters have single atoms or triangles added along the three fold axis, whereas in toroidal clusters gold atoms edge bridge the chair of gold atoms. The **secs** for the two classes of cluster are given at the top and the polyhedral electron count (pec) for each cluster is also shown.

negative charge and the gold atoms in the staples contain  $d^{10} \text{Au}^+$  ions and contribute no electrons for skeletal bonding. Therefore, in the thiolato- cluster  $[\text{Au}_m(\text{SR})_n]$  the skeletal electron count (**sec**) is  $(m-n)$  electrons, i.e. the number of gold 6s valence electrons not involved in the staples, but contributing to the skeletal bonding. In this definition of the **sec** the filled  $5d^{10}$  shells on the gold atoms are ignored. Unfortunately, the **sec** does not define the number of core and staple gold atoms and it is necessary to set up additional constraints *via* a series of simultaneous equations, to establish solutions which are consistent with the formula and the **sec**.<sup>38,39</sup>

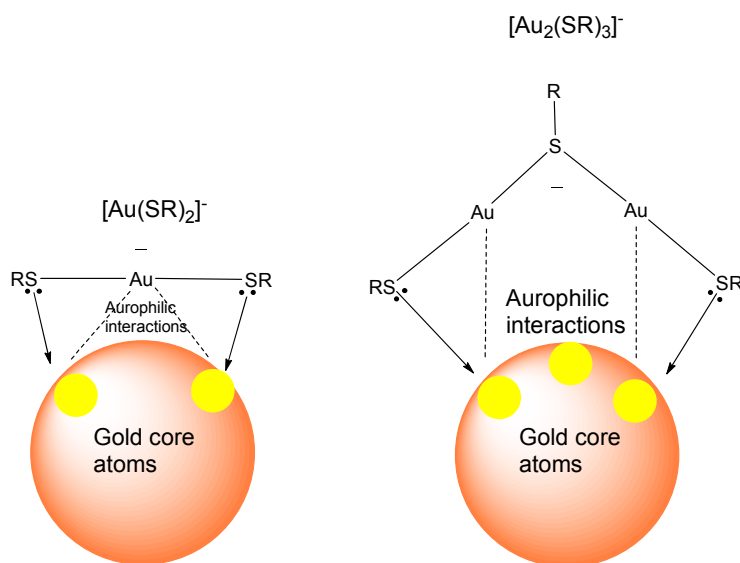


**Figure 5.** Illustration of the divide and protect concept, which has  $[\text{Au}_n(\text{SR})_{n+1}]^+$  “staples” bound to a central core of gold atoms. The  $[\text{Au}_n(\text{SR})_{n+1}]^+$  staples represent examples of ligands constructed from co-ordination complexes of Au(I) with organo-thiolato- ligands, and they are discussed in more detail elsewhere.<sup>33,39</sup>

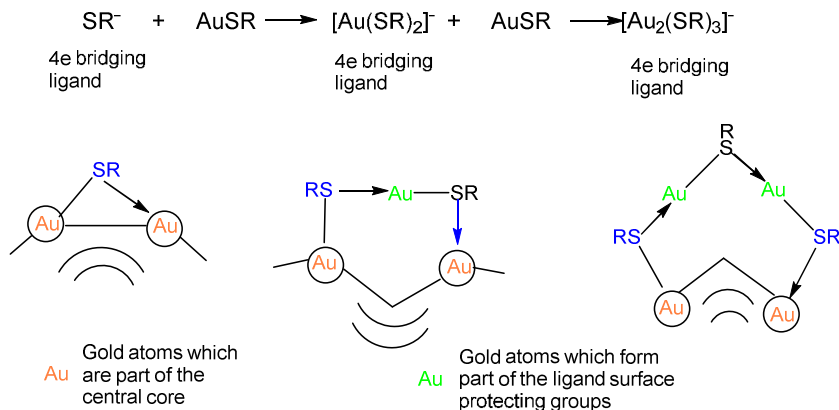


**Figure 6.** Formal electron donating abilities of “staple” ligands. It is also noteworthy that the bite angles vary with the degree of polymerisation of the “staples” and has implications for their ability to span concave and convex surfaces of the core.

Significant theoretical insights into the structures of the organothiolato- gold clusters have been achieved by detailed DFT molecular orbital calculations on specific structures.<sup>31-38</sup> The results have generally been interpreted within the framework of the *jellium model* developed initially to interpret the structures of sodium clusters studied in the gas phase by Knight<sup>40-42</sup> and subsequently adapted to gold phosphine clusters by Mingos.<sup>43-47</sup> The jellium model is essentially a spherically constrained free electron model which leads to the following energy levels  $1s > 1p > 1d > 2s > 1f > 2p > 1g > 2d > 3s > 1h \dots$  *Aufbau* filling of these

energy levels leads to shell closings for 2, 8, 18, 32, 46, 58... electrons.<sup>46</sup> Extensions of Stone's Tensor Surface Harmonic Theory<sup>48-50</sup> to sodium and gold clusters established electronic relationships between the jellium closed shells and sub-shells and cluster geometries. The competing requirements for attaining spherical symmetries and close packing of metal atoms was also explored.<sup>44</sup> Häkkinen<sup>31-37</sup> in his "Gold Superatom" model has satisfactorily attributed the isolation of  $[\text{Au}_{25}(\text{SC}_2\text{H}_4\text{Ph})_{18}]^-$  (icosahedral core with an **sec** of 8 electrons) and  $[\text{Au}_{102}(\text{SC}_6\text{H}_4\text{CO}_2\text{H})_{44}]$  (capped Marks deltahedron core with an **sec** of 58 electrons) to jellium closed shells. The more extensive list of organothiolato- gold and related clusters listed in Table 1 suggests that this application of the jellium model may be an oversimplification. Specifically there are a number of clusters with skeletal electron counts between 8 and 18 (shown in the Table in italics) and this is reminiscent of the spherical-prolate-oblate-spherical series of phosphine gold clusters discussed above. Although, many of the exceptions in Table 1 have prolate geometries the absence of oblate structures suggests that these larger clusters are not generating sub-shells using analogous distortions. In this *Perspective* an alternative model based on icosahedra and cuboctahedra building blocks accounts for the partially filled  $D^\sigma$  sub-shells using a united atom model.

The growth of molecular clusters stabilised by carbonyl, phosphine or organothiolato-ligands is a kinetically controlled process and the growth phase, which proceeds after nucleation, may not necessarily result from the addition of successive spherical shells around a central atom. More facile growth pathways based on the condensation of smaller cluster units may be preferred. Many higher nuclearity metal carbonyl clusters have condensed structures and their closed shell requirements have been rationalised by an extension of PSEPT. Dahl and his co-workers<sup>51-55</sup> have demonstrated that the structures of many carbonyl and phosphine clusters of the later transition metals and the coinage metals are based on the aggregation of icosahedral clusters which come together to form condensed structures with two, three or five-fold symmetries. Teo<sup>56,57</sup> has demonstrated that a series of silver-gold clusters result from vertex sharing of icosahedra. These cluster condensation reactions lead initially to non-spherical clusters, for which the jellium model, based on closed shells may not be applicable. If the low symmetry condensed clusters, formed initially, undergo subsequent annealing processes this may lead to more spherical closed packed structures, which may be interpreted using the jellium model.

The evolution of molecular orbitals connecting two initially separated clusters which progressively merge brings to mind the *united atom model*, whose essential features are summarised in Figure 7.<sup>58-60</sup> On the right hand side the energies and symmetries of two non-interacting neon atoms are shown. The ground states of each atom is  $(1s)^2(2s)^2(2p)^6$  and as the orbital overlaps are turned on by pushing the atoms closer together a removal of the degeneracy results. The orbital splittings are indicated by the symmetry labels appropriate to the  $D_{\infty h}$  point group. The left hand side summarises the corresponding symmetry labels for the atomic orbitals of a single neon atom. The orbitals on the left and right hand sides are correlated using the symmetry constraints of the non-crossing rule. Mulliken and Herzberg<sup>58,59</sup> used an analogous correlation diagram to account for the ground and excited states of the diatomic molecules  $\text{F}_2$ ,  $\text{O}_2$ ,  $\text{N}_2$ ,  $\text{C}_2$  and the results are summarised in Figure 7. The diatomic compression increases the spread of energy levels, and their divergence is consistent with a particle in a sphere (or ellipsoid) analysis.<sup>42,44</sup> Depopulation of the

increasingly antibonding molecular orbitals  $2\sigma_u$  and  $1\pi_g$  results in stronger  $\sigma$  and  $\pi$  bonding and progressively shorter bond lengths. As the internuclear distance is reduced the total number of valence electrons in the diatomic neutral molecules falls from 20 to 12, i.e. Ne...Ne (20), F<sub>2</sub> (18), O<sub>2</sub> (16), N<sub>2</sub> (14), C<sub>2</sub> (12).

**Table 1**  
Examples of gold clusters with cores having five fold symmetry

Formula	sec	No. of metal atoms in core	Description of structure
<i>Icosahedral</i>			
[Au <sub>13</sub> Cl <sub>2</sub> (PR <sub>3</sub> ) <sub>10</sub> ] <sup>3+</sup>	(I)	8	13 Icosahedron
[Au <sub>25</sub> (SR) <sub>18</sub> ] <sup>-</sup>	(II)	8	13 Icosahedron
[Au <sub>13</sub> Ag <sub>12</sub> Br <sub>8</sub> (PR <sub>3</sub> ) <sub>10</sub> ] <sup>+</sup>	(III)	16	25 <i>Pair of vertex sharing icosahedra</i>
[Au <sub>38</sub> (SR) <sub>24</sub> ]	(IV)	14	23 <i>Face sharing icosahedra</i>
[Pt <sub>19</sub> (CO) <sub>17</sub> ] <sup>8-</sup>	(V)	8	19 Interpenetrating pair of icosahedra
[Au <sub>17</sub> Ag <sub>2</sub> Br <sub>8</sub> (PR <sub>3</sub> ) <sub>10</sub> ] <sup>+</sup>	(VI)	10	19 <i>Interpenetrating pair of icosahedra</i>
[Pt <sub>19</sub> (CO) <sub>22</sub> ] <sup>4-</sup>	(VII)	14	19 <i>Pair of face sharing capped pentagonal prisms</i>
<i>Cuboctahedral</i>			
[Au <sub>23</sub> (SR) <sub>16</sub> ] <sup>-</sup>	(IX)	8	15 Biccapped cuboctahedron
[Au <sub>28</sub> (SR) <sub>20</sub> ]	(VIIIa)	8	20 <i>Interpenetrated cuboctahedra</i>
[Au <sub>30</sub> (SR) <sub>18</sub> S]	(VIIIb)	10	20 <i>Interpenetrated cuboctahedra</i>
[Au <sub>36</sub> (SR) <sub>24</sub> ]	(X)	12	24 <i>Tetrahedron of cuboctahedra</i>
<i>Other geometries</i>			
[Au <sub>14</sub> (PR <sub>3</sub> ) <sub>10</sub> ] <sup>4+</sup>	(XI)	10	14 <i>Linked tricapped tetrahedra</i>
[Au <sub>20</sub> (PPhpy) <sub>2</sub> ] <sub>10</sub> Cl <sub>4</sub> <sup>2+</sup>	(XII)	14	20 <i>Pair of icosahedra-minus-edge</i>

Entries in italics refer to examples which do conform to a simple jellium model analysis.

**References:** (I) C.F. Briant, B.R.C. Theobald, J.W. White, L.K. Bell, D.M.P. Mingos and A.J. Welch, *J. Chem. Soc. Chem. Commun.*, 1981, 201; (II) M.W. Heaven, A. Dass, P.S. White, K.M. Holt and R.W. Murray, *J. Am. Chem. Soc.*, 2008, **130**, 3754; (III) B. K. Teo and K. Keating, *J. Am. Chem. Soc.*, 1984, **106**, 2224, B.K. Teo *Polyhedron*, 1988, 2317; (IV) H. Qian, W.T. Eckenhoff, Y. Zhu, T. Pintauer and R. Jin, *J. Am. Chem. Soc.*, 2010, **132**, 8280; (V) C. Femoni, M.C. Iapucci, G. Longoni, S. Zacchini and S. Zarra, *J. Am. Chem. Soc.*, 2011, **133**, 2406; (VI) K. Nunokawa, M. Ito, T. Sunahara, S. Onaka, T. Ozeki, H. Chiba, Y. Funahashi, H. Masuda, T. Yonezawa, H. Nishihara, M. Nakamoto and M. Yamamoto, *J. Chem. Soc. Dalton Trans.*, 2005, 2726; (VII) D.M. Washecheck, D.J. Wucherer, L.F. Dahl, M. Ceriotto, M. Sansoni and P. Chini, *J. Am. Chem. Soc.*, 1979, **101**, 6110; (VIII) C. Zeng, A. Das, N.L. Rosi and R. Jin, *J. Phys. Chem. C*, 2008, **112**, 14221; (IX) A. Das, T. Li., K. Nobusada, C. Zeng, N. L. Rosi and R. Jin, *J. Am. Chem. Soc.*, 2013, **135**, 18264; (X) C.J. Zeng, H.F. Qian, T. Li, *Angew. Chem. Int. Ed.*, 2012, **51**, 13114; (XI) B.S. Guttrath, I.M. Oppel, O. Presly, I. Beljakov, V. Meded, W. Wenzel and U. Simon, *Angew. Chem. Int. Ed.*, 2013, **52**, 3529; (XII) X.K. Wan, Z.W. Lin and Q.M. Wang, *J. Phys. Chem. B*, 2004, **108**, 12259.

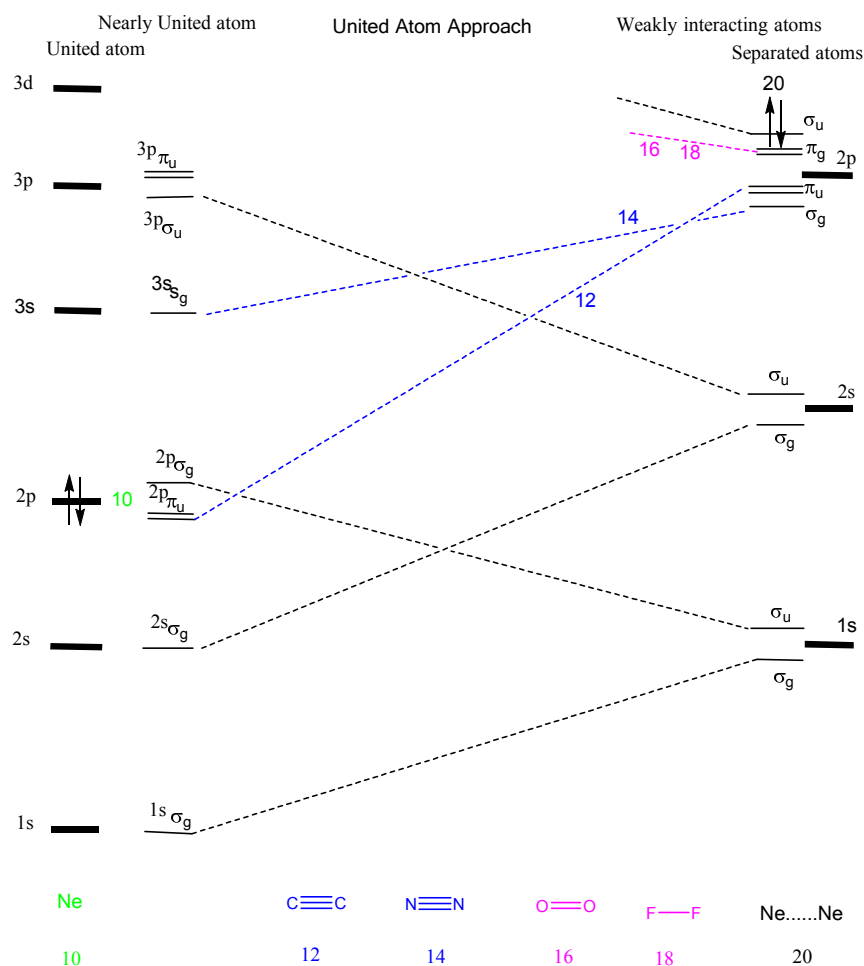


**Figure 7.** Summary of orbital correlations in the united atom approach developed by Mulliken<sup>59</sup>

Following Mulliken's methodology,<sup>59</sup> the molecular orbitals of condensed clusters of gold atoms may similarly be described in terms of linear combinations of the separated cluster molecular orbitals. An isolated icosahedral or cuboctahedral gold cluster is sufficiently spherical that its skeletal molecular orbitals have the same nodal properties as the atomic orbitals of a main group atom and if spherical symmetry labels are used rather than point group symmetry labels the bonding skeletal molecular orbitals are designated as  $S^\sigma$  and  $P^\sigma$  and the antibonding skeletal molecular orbitals  $D^\sigma$  and  $F^\sigma$  (see Figure 1). In aggregates of gold clusters linear combinations of the pseudo-spherically symmetric bonding skeletal molecular orbitals ( $S^\sigma$  and  $P^\sigma$ ) may be symmetry matched and combined in an analogous manner to that described above, and in a way that is familiar to chemists.<sup>60</sup>

Figure 8 illustrates the evolution of the bonding skeletal molecular orbitals as a pair of centred  $M_{13}$  metal icosahedral clusters are compressed together, i.e. following "a united cluster approach". In such a correlation diagram the non-crossing rule symmetry restrictions applying to spherical atoms are applied as in Figure 7. The absence of radial nodes  $L^\sigma$  for the bonding orbitals in a single shell cluster leads to a slightly simpler correlation diagram than

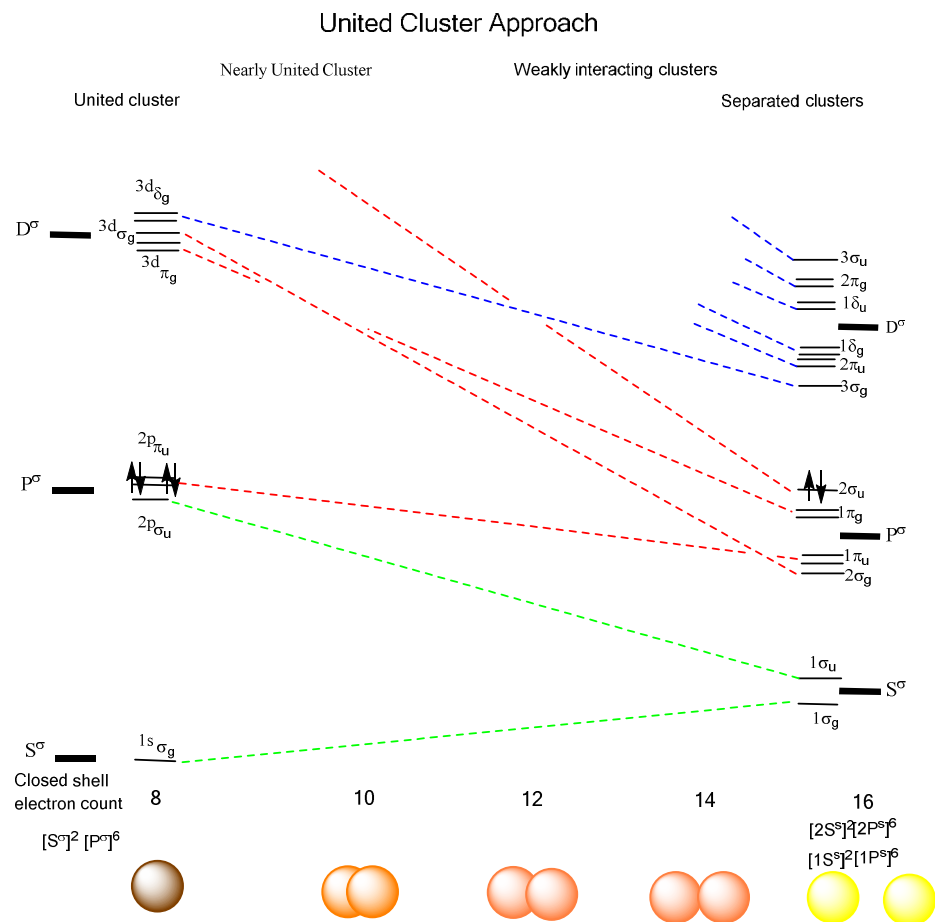


**Figure 8.** The application of the *united cluster approach* to gold clusters. The molecular orbitals of the separated clusters are shown on the right and those of united cluster on the left. The degree of interpenetration between the clusters increases from right to left and is indicated schematically by the overlapping spheres shown at the bottom.

that commonly constructed for diatomic molecules. The relative ordering of the atomic and molecular orbitals differ in detail, i.e.  $1s > 2s > 2p > 3s > 3p > 3d$  for a hydrogen like atom and  $S^{\sigma} > P^{\sigma} > D^{\sigma} > F^{\sigma}$  for gold clusters. The united cluster correlation diagram in Figure 8 leads to the following energy level ordering  $1\sigma_g > 1\sigma_u > 1\pi_u > 2\sigma_g > 1\pi_g > 2\sigma_u$  along the majority of the compression co-ordinate. The cross-over between  $2\sigma_g$  and  $1\pi_u$  results because the former correlates with  $D^{\sigma}$  and the latter with  $P^{\sigma}$  in the united cluster.

The overall energy dispersion of molecular orbitals in the united cluster correlation diagram is governed primarily by the inter-cluster overlaps of molecular orbitals<sup>60</sup> with matching pseudo-spherical symmetries, i.e.  $S^{\sigma}$  and  $S^{\sigma}$  and  $P^{\sigma}$  and  $P^{\sigma}$  and the symmetry allowed mixings between  $S^{\sigma}$  and  $P^{\sigma}$  represent a second-order effect. The overlap integrals and corresponding resonance integrals between the metal clusters are smaller than those involving diatomic molecules of the second row elements. Therefore, the dispersion of energy levels will be correspondingly smaller and the *aufbau* fillings in Figure 8 are likely to be more dependent on the metal atoms at the interfaces of the clusters and the bridging ligands.

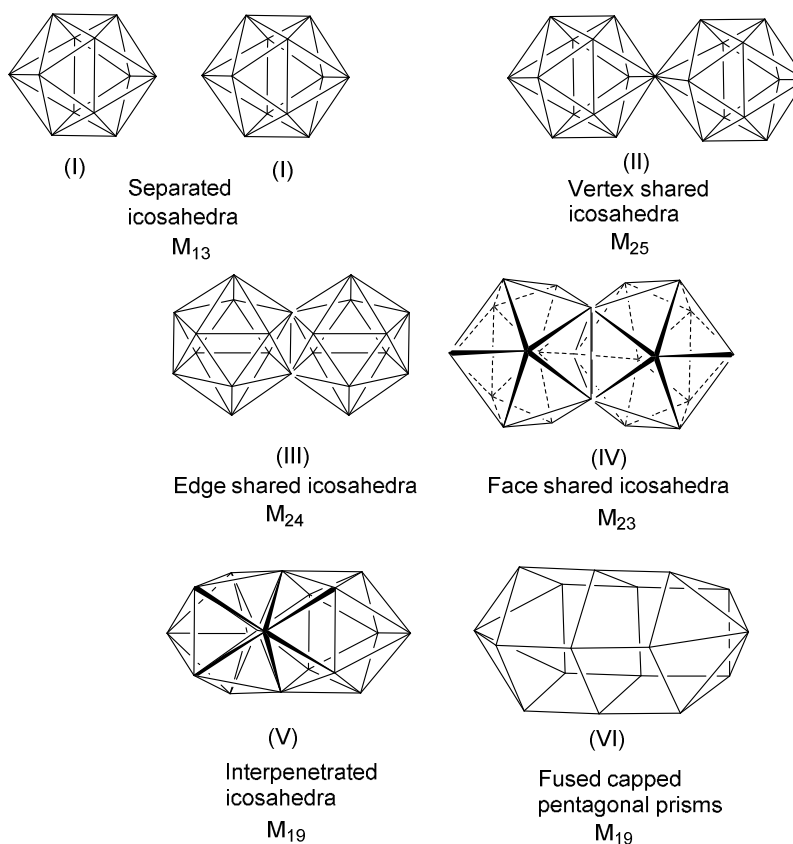


**Figure 9.** The generation of condensed icosahedra based on vertex, edge and face sharing is illustrated and this corresponds successively to a compression of the pair of clusters to form eventually a united spherical cluster. In the interpenetrated icosahedral example (V) the two icosahedra share 20 faces and two atoms which become interstitial (see Figure 10) and this may be contrasted with the fused capped pentagonal prism (VI) which has the same number of metal atoms but a more prolate structure because the central pentagonal layers are not staggered.

The extension of Mulliken's united atom approach for diatomics to clusters of gold based on icosahedra or cuboctahedra needs to be accompanied by some discussion of the differences between an atom and a cluster dimer. The analogue of a compression of a diatomic molecule is an increased interpenetration of the two clusters by the progressive sharing of more vertices. When a pair of icosahedral clusters increasingly share vertices, edges and faces the total number of metal atoms decreases as does the total volume. They also become progressively less prolate and more spherical (see Figure 9). (Reference 39 describes a methodology for defining mathematically the sphericity of polyhedra and condensed polyhedra.) Greater interpenetration may be achieved by sharing internal faces as shown schematically in Figure 10. Two icosahedral  $M_{12}$  non-centred metal clusters may be conjoined together to form an  $Au_{19}$  cluster with 2 interstitial and 17 surface gold atoms by

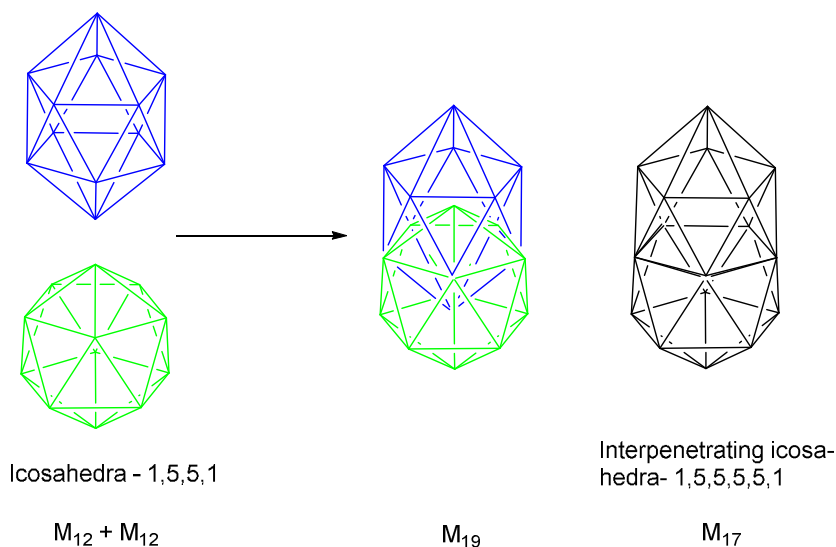


**Figure 10** . Interpenetration of two icosahedral  $M_{12}$  polyhedra by sharing a common pentagonal face leading to an outer shell of 17 vertices and two interstitial atoms.

sharing a common pentagonal internal face. The resultant polyhedron retains a five-fold symmetry axis which coincides with the direction of approach.

As Stone has shown<sup>48,49,44</sup> the relative energies of the  $L^\sigma$  skeletal molecular orbitals in clusters where s-s orbital interactions predominate are determined primarily by the number of nodal planes. In the isolated icosahedron,  $S^\sigma$  has no angular nodes and  $P^\sigma$  a single angular node. When the icosahedra are brought together the dispersion of the in-phase and out-of-phase combinations depends on the number of additional next neighbours generated by the polyhedral condensation process and the strength of the overlaps. As the icosahedra are condensed more fully the interstitial atoms are brought closer together and have an important influence on the energies of the orbitals. Figure A in the Appendix illustrates the evolution of molecular orbitals in the icosahedrally based clusters (III) to (V) of Figure 9. The evolution of  $S^\sigma$  and  $P^\sigma$  molecular orbitals as the condensation process proceeds, which was introduced in a general way in Figure 8, is reproduced for specific examples. At one limit (separated clusters) there are 8 skeletal molecular orbitals ( $1S^\sigma$  and  $1P^\sigma$  and  $2S^\sigma$  and  $2P^\sigma$ ) and at the other (united cluster) there are 4 strongly bonding skeletal molecular orbitals ( $1S^\sigma$  and  $1P^\sigma$ ) and four antibonding ( $2S^\sigma$  and  $2P^\sigma$ ). The molecular orbitals which show the largest variations with condensation are  $1\sigma_u$ ,  $1\pi_g$  and  $2\sigma_u$ , which have a nodal plane between the two halves of the resultant cluster. The relevant molecular orbitals for the vertex and edge sharing icosahedra are illustrated in Figures B and C of the Appendix. The least stable molecular orbital is  $2\sigma_u$  and it matches the lUMO in diatomic molecules such as  $F_2$  and  $Cl_2$ .

Therefore, interpenetration of polyhedra provides the equivalent of compression for simple diatomic molecules. Just as the increased compression in diatomic molecules leads to reduced total electron counts (see Figure 7) so the greater interpenetration of polyhedral clusters leads to a wider dispersion of energy levels and the preference for clusters with smaller total electron counts. This effect is synergic since the reduced electron count also results in the depopulation of antibonding skeletal molecular orbitals. It follows that there is

a correlation between interpenetration and the skeletal electron counts (**sec**) in condensed clusters.

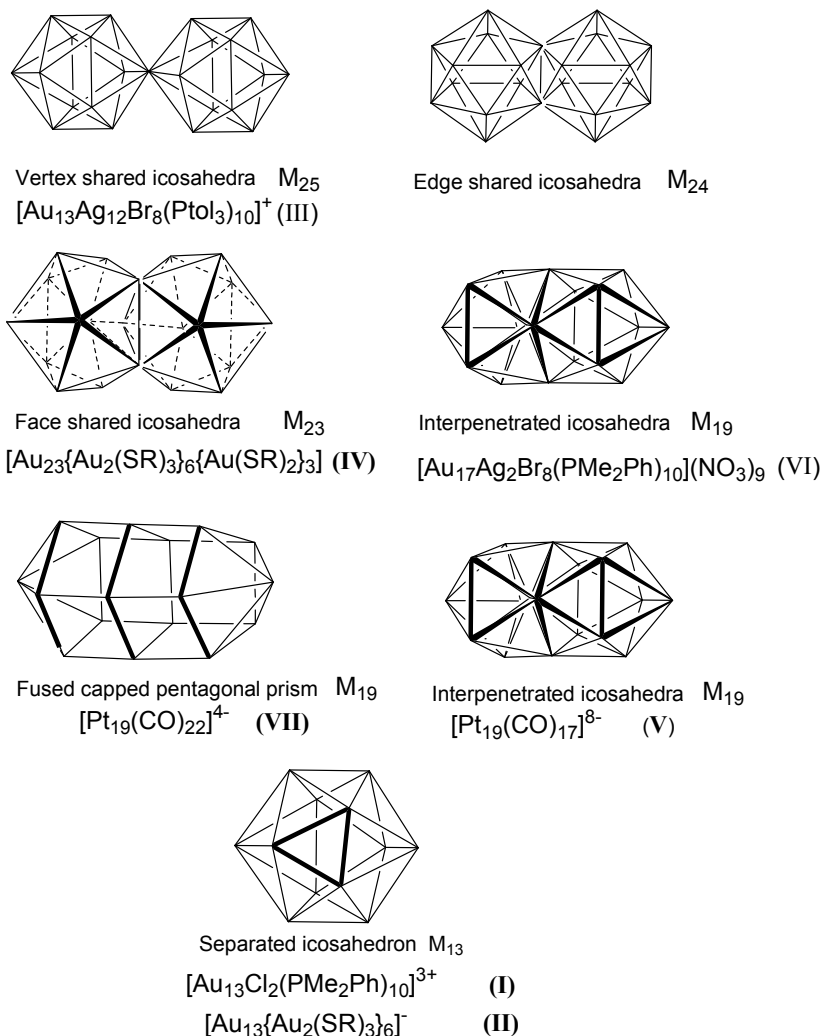


**Figure 11.** Examples of gold and platinum clusters with increased interpenetration. The skeletal electron counts for the clusters (**sec**) are given in Table 2.

Figure 11 illustrates specific examples of the structures of clusters based on interpenetrated pairs of icosahedra and Table 2 summarises the occupied energy levels. As the degree of interpenetration increases the **secs** given in Table 2 fall from 16 to 8 and may be interpreted by an *aufbau* filling of the energy levels in Figure 8 and summarised in Table 2. The gold-silver cluster (III) which has a pair of centred icosahedra sharing a vertex is characterised by a **sec** of 16 and the inter-icosahedral interactions are sufficiently weak that the 8 molecular orbitals originating from the  $S^\sigma$  and  $P^\sigma$  molecular orbitals of the isolated icosahedra are fully occupied. Teo<sup>56,57</sup> has studied in great detail the structures of several gold-silver icosahedral

**Table 2**  
***Aufbau* filling of molecular orbitals in condensed icosahedral clusters**

<b>Cmpd</b>	<b>sec</b>	<b>Occupation of energy levels in Fig. 8 and A</b>	<b>Description of structure</b>
<b>(III)</b>	16	$(1\sigma_g)^2 (1\sigma_u)^2 (1\pi_u)^4 (2\sigma_g)^2 (1\pi_g)^4 (2\sigma_u)^2$	Vertex linked Au/Ag icosahedra
<b>(IV)</b>	14	$(1\sigma_g)^2 (1\sigma_u)^2 (1\pi_u)^4 (2\sigma_g)^2 (1\pi_g)^4 (2\sigma_u)^0$	Face sharing icosahedra
<b>(VI)</b>	14	$(1\sigma_g)^2 (1\sigma_u)^2 (1\pi_u)^4 (2\sigma_g)^2 (1\pi_g)^4 (2\sigma_u)^0$	Ag/Au interpenetrated icosahedra
	10	$(1\sigma_g)^2 (1\sigma_u)^2 (1\pi_u)^4 (2\sigma_g)^2 (1\pi_g)^0 (2\sigma_u)^0$	
<b>(V)</b>	8	$(1\sigma_g)^2 (1\sigma_u)^2 (1\pi_u)^4 (2\sigma_g)^0 (1\pi_g)^0 (2\sigma_u)^0$	Interpenetrating Pt icosahedra
<b>(I), (II)</b>	S	$(S_\sigma)^2 (P_\sigma)^6$	Single icosahedron

clusters with shared vertices. Linear, triangular and tetrahedral linked geometries with **secs** of  $8n$  (where  $n = 2-4$ ) have been structurally characterised by his group. Pignolet<sup>23</sup> has studied related platinum-silver-gold clusters, e.g.  $[\text{Au}_{10}\text{Ag}_{13}\text{Pt}_2\text{Cl}_7(\text{PR}_3)_{10}]$  which has an **sec** of 16.

For a pair of icosahedra sharing a triangular face an **sec** of 14 is predicted and observed in  $[\text{Au}_{38}(\text{SR})_{24}]$  (IV). When a pair of icosahedra are interpenetrated as shown in Figure 11, alternative *aufbau* possibilities may result depending on the strength of the intercluster interactions:  $(1\sigma_g)^2 (1\sigma_u)^2 (1\pi_u)^4 (2\sigma_g)^2 (1\pi_g)^4 (2\sigma_u)^0$  results in a **sec** of 14 in the gold/silver cluster (VI) and  $(1\sigma_g)^2 (1\sigma_u)^2 (1\pi_u)^4 (2\sigma_g)^0 (1\pi_g)^0 (2\sigma_u)^0$  is consistent with **sec** of 8 observed in the platinum carbonyl cluster (V). In  $[\text{Au}_{13}\text{Ag}_{12}\text{Br}_8(\text{PR}_3)_{10}]^+$  (VI) the presence of silver atoms at the intersection of the interpenetrated icosahedra at the adjacent pentagonal faces results in weaker metal-metal interactions than in the platinum cluster (V). This leads to a population of  $2\sigma_g$  and  $1\pi_g$ , which are not occupied in the platinum cluster. The analysis summarised in Figure 11 and Table 2 highlights two missing members in the series:  $M_{24}$  with **sec** of 14 and with two centred icosahedra sharing an edge and an interpenetrated cluster with **sec** of 10, i.e.  $(1\sigma_g)^2 (1\sigma_u)^2 (1\pi_u)^4 (2\sigma_g)^2 (1\pi_g)^0 (2\sigma_u)^0$ . The predictive ability of the model may therefore be determined by future structural studies.

The closely related platinum carbonyl clusters (V) and (VII) both have 19 metal atoms and a five-fold symmetry axis. The former has successive five atom layers with eclipsed and staggered arrangements. The staggered arrangements lead to stronger metal-metal interactions and a more compressed structure and this probably accounts for the alternative **secs** of 14 and 8 noted for these related platinum clusters.<sup>39</sup>

It is noteworthy that the examples shown in this Figure and Table 1 have been drawn widely and examples of gold phosphine clusters, platinum carbonyl clusters and gold thiolato- clusters have been included. It has been commonly assumed in the literature that these three classes of clusters are quite distinct and require alternative models. The present analysis, although it is based primarily on symmetry concepts, suggests that similar bonding principles apply to all of these compounds, which share the common characteristic of being based on icosahedra and condensed icosahedra. Furthermore it makes the important point that as the condensed clusters become progressively more interpenetrated and spherical the **secs** asymptotic approach that predicted from a jellium model. Thus the interpenetrated cluster (V) has the same **sec** as the single shell clusters (I) and (II) although the latter has two and the

latter only a single interstitial atom. It follows more generally that the jellium model cannot be interpreted in terms of spherical shells of atoms surrounding a single metal atom.

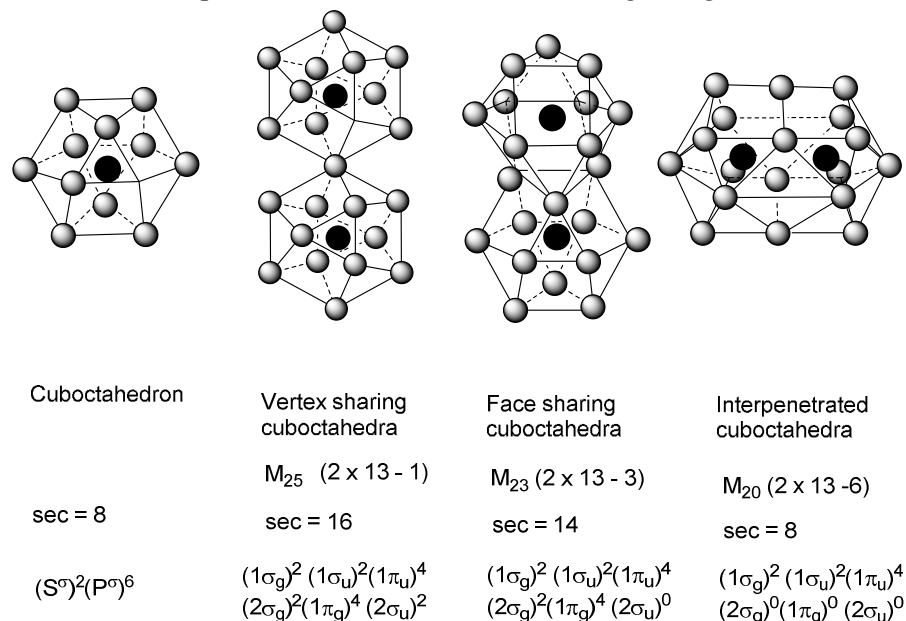


**Figure 12.** Condensation of cuboctahedral clusters *via* vertex and face sharing and interpenetration .

It has been previously noted that the skeletal molecular orbitals in centred icosahedral and cuboctahedral  $Au_{13}$  clusters are very similar (see Figures 1a and 1b) and the former is generally more stable because of the greater number of gold-gold contacts. However, the energy difference is relatively small and the situation may be reversed by gold-ligand bonding effects. The united cluster approach developed for centred icosahedra may therefore be extended to clusters based on the condensation and interpenetration of cuboctahedron. The results are summarised in Figure 12. Although, no examples of gold thiolato- or phosphine clusters have been shown to contain a cuboctahedron  $Au_{13}$  at its core  $[Au_{23}(SR)_{16}]^-$  has a bicapped cuboctahedron which is consistent with the presence of a **sec** of 8.<sup>61</sup> The capping principle developed 40 years ago<sup>5,6</sup> suggests that a capped polyhedron has the same number of skeletal bonding molecular orbitals as the parent polyhedron as long as the frontier orbitals of the capping atoms do not produce linear combinations which do not match the skeletal bonding molecular orbitals of the parent. In  $[Au_{23}(SR)_{16}]^-$  the two capping atoms are located along the three fold axis and therefore generate  $S^\sigma$  and  $P^\sigma(z)$  which match the bonding skeletal molecular orbitals and therefore the **sec** remains 8.<sup>61,62</sup>  $[Au_{28}(SR)_{20}]$  (VIII) has as a kernel a pair of interpenetrated pair of cuboctahedra and therefore is the cuboctahedral analogue of (V) and an identical **sec** of 8. In common with (V) this cluster conforms to the jellium model although it does not have a spherical structure with a single atom at its origin. For the interpenetrated icosahedra summarised in Table 2 an **sec** of 10 associated with the *aufbau* filling of  $2\sigma_g$  may also be possible and  $[Au_{30}(S^tBu)_{18}S]$  which has interpenetrated cuboctahedra represents a specific example of such a cluster.<sup>63</sup>

The smaller number of skeletal molecular orbitals in gold clusters compared with metal carbonyl clusters of the earlier transition metals, which have radial and tangential sets of molecular orbitals, means that the application of the capping principle is less

straightforward for clusters with only radial MOs. Specifically, multiple capping leads to the formation of additional linear combinations and if they do not match the bonding MOs of the parent then additional MOs result. For clusters based on the icosahedron and cuboctahedron, if the capping atom 6s orbitals generate  $x$  linear combinations with  $D^\sigma$  pseudo-spherical symmetries, then  $x$  additional skeletal MOs result. This aspect will be discussed more fully in a subsequent paper<sup>64</sup>, however for completeness sake we note the extensive recent experimental work in this area particularly by Konishi and co-workers<sup>65-68</sup> and some of the theoretical studies which have previously covered this topic.<sup>5,6,45</sup>

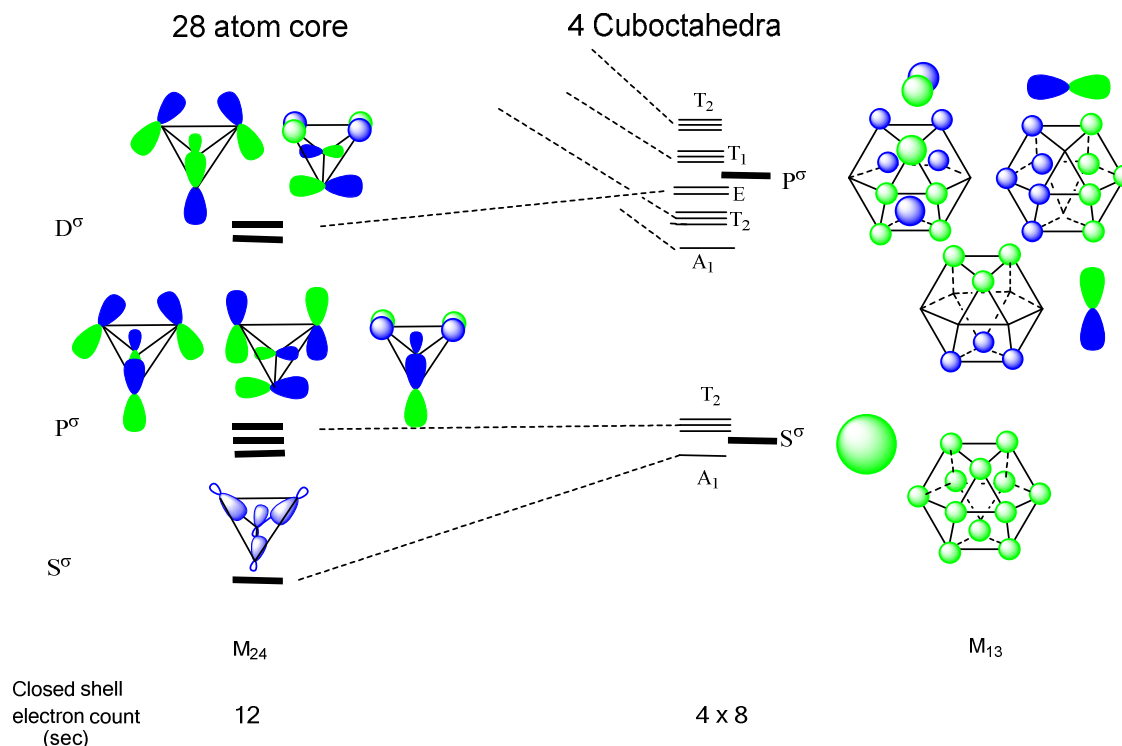


**Figure 13.** Construction of the skeletal molecular orbitals in a tetrahedron of cuboctahedra.

The discussion above has centred on the development of a symmetry based model for pairs of spherical clusters with varying degrees of interpenetration. However, the same principles may be applied to developing an understanding of the skeletal molecular orbitals in larger clusters which may be viewed as molecules of clusters.<sup>60</sup> For example, four centred  $M_{13}$  cuboctahedra may be brought together in a tetrahedral fashion to generate an  $M_{24}$  cluster. In atomic terms this corresponds to forming a tetrahedral  $P_4$  cluster and Figure 13 illustrates the symmetry analysis for formation of the frontier orbitals from those of the atomic fragments.<sup>11</sup> Main group tetrahedral  $M_4$  clusters are characterised by 6 bonding skeletal molecular orbitals and therefore extension of this analysis to the  $S^\sigma$  and  $P^\sigma$  molecular orbitals of a cuboctahedron, which suggests that the resultant  $M_{36}$  cluster will be associated with an **sec** of 12. This geometry and **sec** has been established for  $[Au_{36}(SR)_{24}]$ , i.e.  $[Au_{24}\{Au_2(SR)_3\}_4(SR)_{12}](X)$ .<sup>69</sup>

Although the symmetry analysis developed above has been illustrated using icosahedral and cubo-octahedral clusters as building blocks, the approach may also be applicable to other clusters which do not conform to the jellium model. For example,  $[\text{Au}_{20}(\text{PPhy}_2)\text{Cl}_4]^{2+}$  (XII) has a structure derived from an icosahedron with a missing edge (see Figure 14).<sup>70</sup> Two 10 vertex *arachno*-icosahedra condense by sharing the vertices as shown in Figure 14 and the addition of two interstitial gold atoms leads to the  $\text{Au}_{20}$  cluster illustrated in the centre of the Figure. Alternatively it may be viewed as a pair of interpenetrating icosahedra which share two internal vertices and lose two pairs of edges from the original polyhedron as shown on the right hand side of Figure 14. This cluster has a skeletal electron count of 14 electrons  $[(1\sigma_g)^2 (1\sigma_u)^2 (1\pi_u)^4 (2\sigma_g)^2 (1\pi_g)^4 (2\sigma_u)^0]$ .

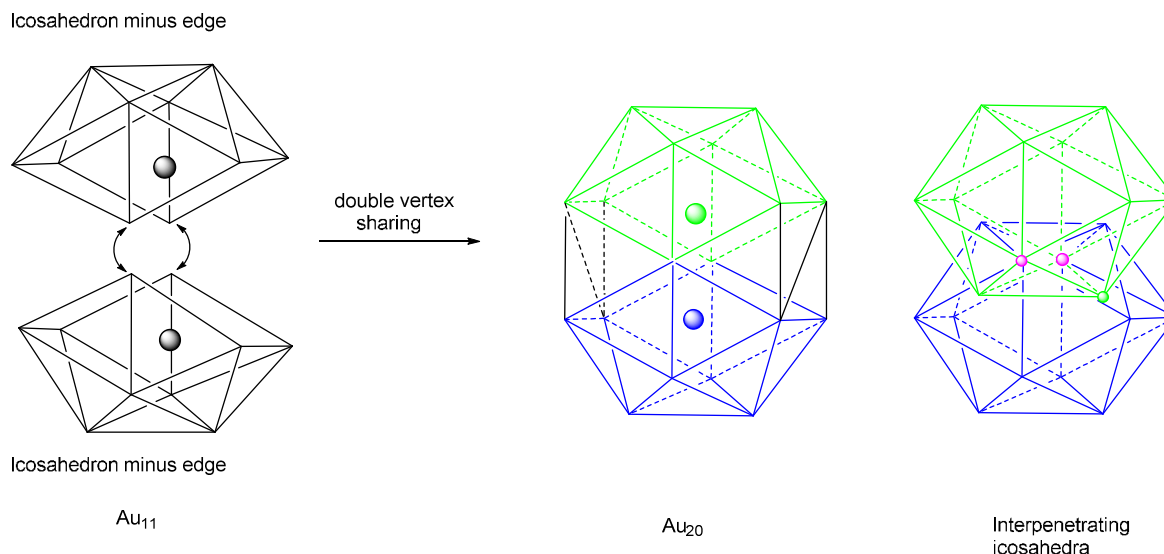


**Figure 14.** Schematic representation of the interpenetration or condensation processes leading to the observed skeletal structure of  $[\text{Au}_{20}(\text{PPhy}_2)\text{Cl}_4]^{2+}$ . The structure may be viewed either as a pair of condensed clusters derived from icosahedra minus an edge or the interpenetration of two icosahedra with the loss of two edges shown in green and blue and the sharing a second pair of vertices shown in red.

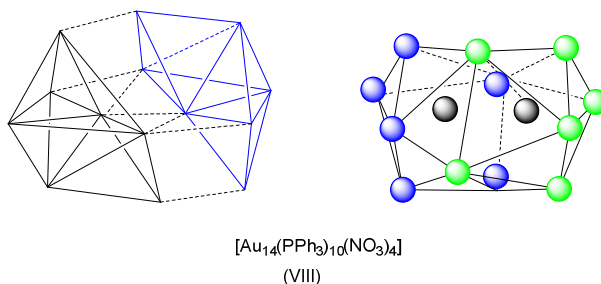


**Figure 15.** The description of  $[\text{Au}_{14}(\text{PPh}_3)_8(\text{NO}_3)_4]$  as a pair of a bicapped trigonal bipyramids linked by a strong Au-Au bond shown by the black spheres.

Simon et al<sup>71</sup> have recently reported the structure of  $[\text{Au}_{14}(\text{PPh}_3)_8(\text{NO}_3)_4]$  which according to the usual electron counting paradigms is a 10 electron cluster and the jellium model would suggest a  $1s^2 1p^6 1d^2$  ground state, based on a partially filled d shell. He has proposed that the presence of the nitrato- ligands leads to a superatom jellium cluster by effectively

withdrawing 2 skeletal electrons. However, such an electron transfer is unprecedented in this area of cluster chemistry. Within united cluster model the cluster may be viewed as a pair of tricapped tetrahedral sharing vertices as illustrated in Figure 15 and the observed *sec* of 10 is consistent with a  $(1\sigma_g)^2 (1\sigma_u)^2 (1\pi_u)^4 (2\sigma_g)^2 (1\pi_g)^0 (2\sigma_u)^0$  configuration.

The structure of  $[\text{Au}_{20}\{\text{SPh-}^t\text{Bu}\}_{16}]$  has been recently reported<sup>72</sup> and shown to have a  $[\text{Au}_7]^{3+}$  kernel based on a pair of vertex sharing tetrahedral, with  $\{\text{Au}_8(\text{SR})_8\}$ ,  $\{\text{Au}(\text{SR})_2\}_2$  and  $\{\text{Au}_3(\text{SR})_4\}$  staples. Since a tetrahedral cluster is associated with an  $[\text{S}^\sigma]^2$  closed shell vertex sharing leads to an analogous situation to that noted above for a pair of silver/gold icosahedra sharing a vertex (III),  $[1\text{S}^\sigma]^2[2\text{S}^\sigma]^2$  and a *sec* of 4.

## Conclusions

In the 1970s Ken Wade initiated a series of papers which addressed the relationships between the structures of clusters and their skeletal electron counts,<sup>1-5</sup> which complemented the Valence Shell Electron Pair Model for simple main group molecules. Both models related the molecular geometries to the number of valence electron pairs and together provide an important pedagogical introduction to inorganic structural chemistry. This approach was initially extended to gold phosphine clusters in the mid 1970s<sup>15</sup> and not only rationalised those structures which were known at the time, but also predicted some new ones. Forty years on the basic methodology still has value for developing a general conceptual model. It retains unifying and pedagogical strengths and represents a fitting way to mark Ken Wade's imagination and ability to see patterns in structures, which had been missed by many distinguished theoretical chemists. The detailed electronic structures of metal clusters will eventually be tackled using increasingly accurate DFT calculations, but the presence of conceptual models which understanding the kernel structures and provide a rational basis for trying new synthetic routes will remain valuable for new generations of chemists.

The following general conclusions have resulted from the analysis presented in this review:

1. Initially it was thought that phosphine and thiolato- clusters of gold belonged to different classes, but it has become apparent that once the staple ligands of the thiolato- clusters are defined, their cluster cores follow the same bonding principles. Since the staples  $[\text{Au}_m(\text{SR})_{m+1}]^-$  ( $m = 0, 1, 2, 3, \dots$ ) are all 4-electron donors and the linear S-Au-S moieties are associated with 14 valence electrons and a formal  $d^{10}$  shell at the gold atoms, the number of skeletal electrons (*sec*) in  $[\text{Au}_m(\text{SR})_n]$  is  $m - n$ .
2. Gold phosphine and thiolato- clusters do not strictly follow the jellium closed shell requirements and non-spherical structures lead to sub-shells and electron counts which lie between those predicted by the jellium model, i.e. partially filled shells. The partial filling invariably involves an even number of electrons.
3. For single shell clusters this results in spherical, prolate, oblate, spherical sequences of structures, which can be related to 2, 4, 6, 8 electrons filling sub-shells in an *aufbau* fashion. The choice of structures which satisfy the shape and maximisation of the number of nearest neighbours is consistent with the observed structures.
4. For polyspherical clusters the electronic structures may be interpreted using an extension of the united atom approach developed for simple diatomics by Mulliken.

Using the pseudo-spherical symmetry labels for the icosahedron and cuboctahedron it is possible to generate LCAOs which resemble those for the united atom and the compression co-ordinate is represented by increased interpenetration of the icosahedra or cuboctahedra. Increasing interpenetration is achieved *via* vertex, edge and face sharing. The closed shell requirements of the resulting clusters may be understood by *aufbau*-filling of the sub-shells generated by the *united cluster model*.

5. The resulting sub-shell fillings are associated with 8, 10, 12, 14 and 16 electrons and specific examples of clusters which conform to this analysis have been presented. Missing members of the series represent predictions and hopefully will stimulate further research.
6. The most interpenetrated structures have a  $(1\sigma_g)^2 (1\sigma_u)^2 (1\pi_u)^4$  closed shell which corresponds to a jellium filled shell  $(S^\sigma)^2 (P^\sigma)^6$  although they have two metal atoms at the centre of the cluster and therefore do not follow a simple geometric growth pattern based on building successive shells around a single atom.
7. The building up of larger three dimensional clusters with more complex structures may also developed by taking linear combinations of the  $S^\sigma$  and  $P^\sigma$  cluster molecular orbitals in an analogous way to that developed previously for the 2s and 2p atomic orbitals in boron and carbon clusters. The *molecules in clusters* approach has been illustrated for  $[\text{Au}_{36}(\text{SR})_{24}]$  which has an  $M_{24}$  core based on a tetrahedron of cuboctahedra (X).

Those readers interested in a fuller discussion of gold clusters, colloids and nanoparticles may wish to read reviews from leading experts in two recently published volumes.<sup>73,74</sup>

## Appendix

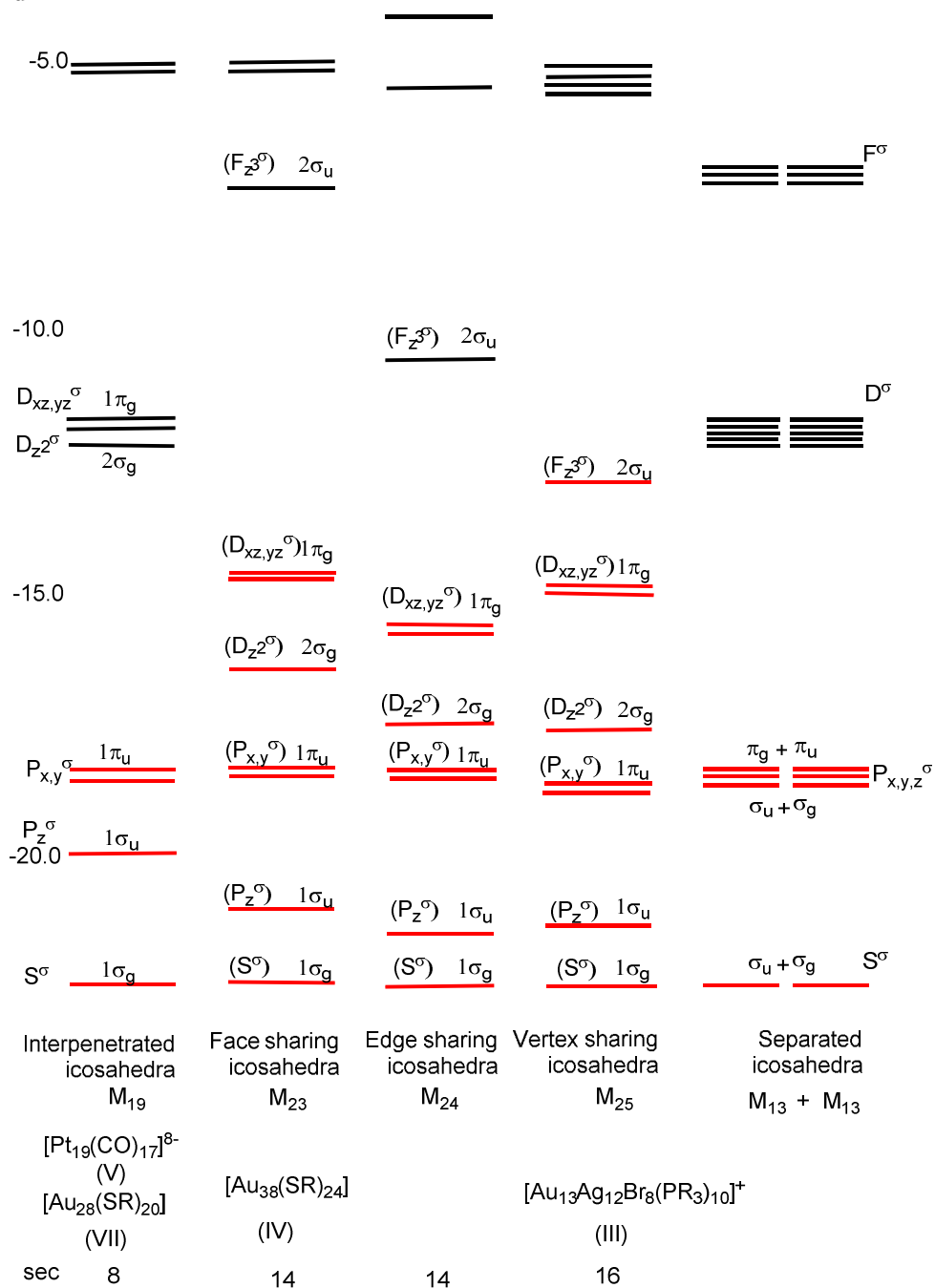


**Figure A .** Calculated orbital energies for the evolution of skeletal molecular orbitals for a pair of centred icosahedra which share vertices, edges and faces based on an extension of the united atom approach. The occupied molecular orbitals are shown in red. The skeletal electron count (**sec**) indicates the number of electrons occupying the orbitals in red. For gold clusters the 5d electrons have been excluded from this electron count and **sec** reflects the number of 6s electrons participating in skeletal bonding.

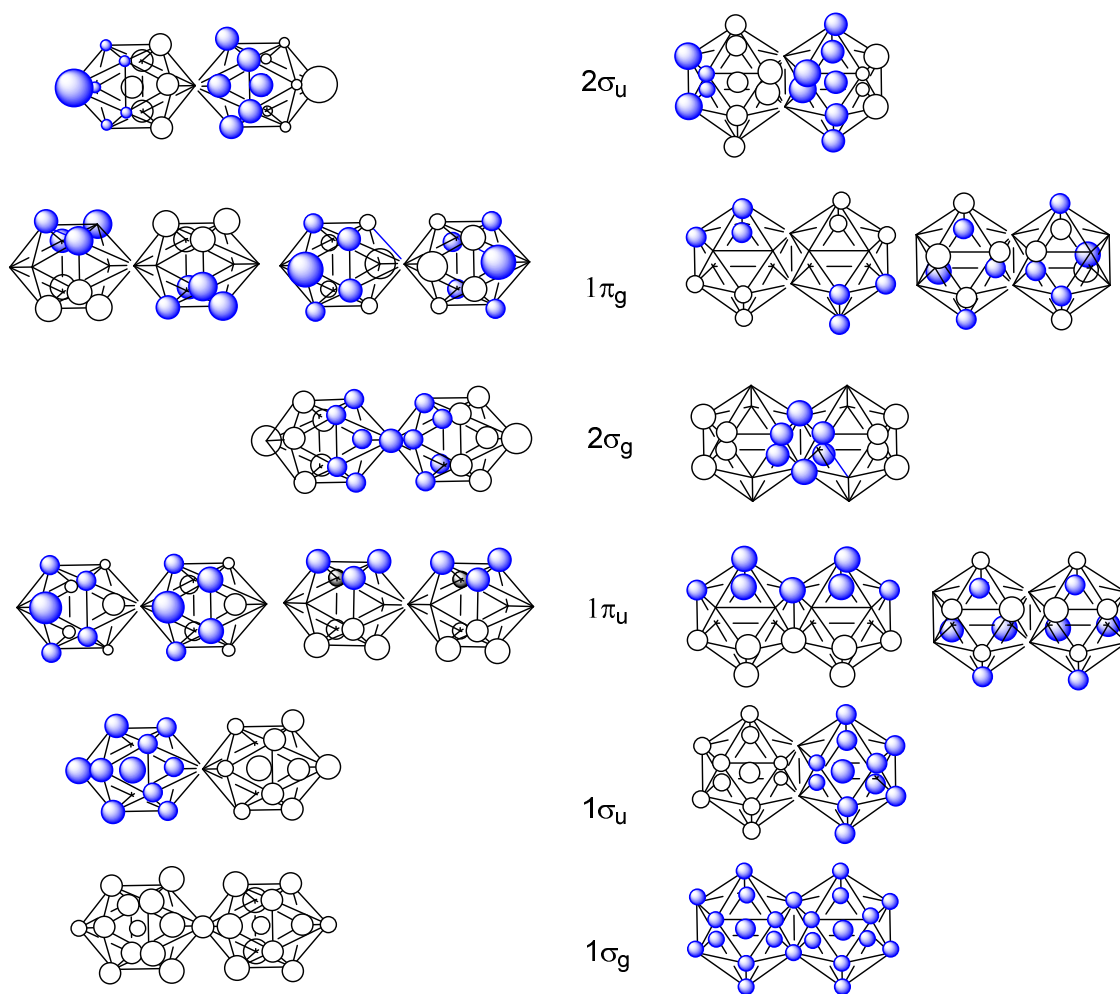


**Figure B.** Schematic illustration of the skeletal molecular orbitals of icosahedra sharing a vertex or an edge.

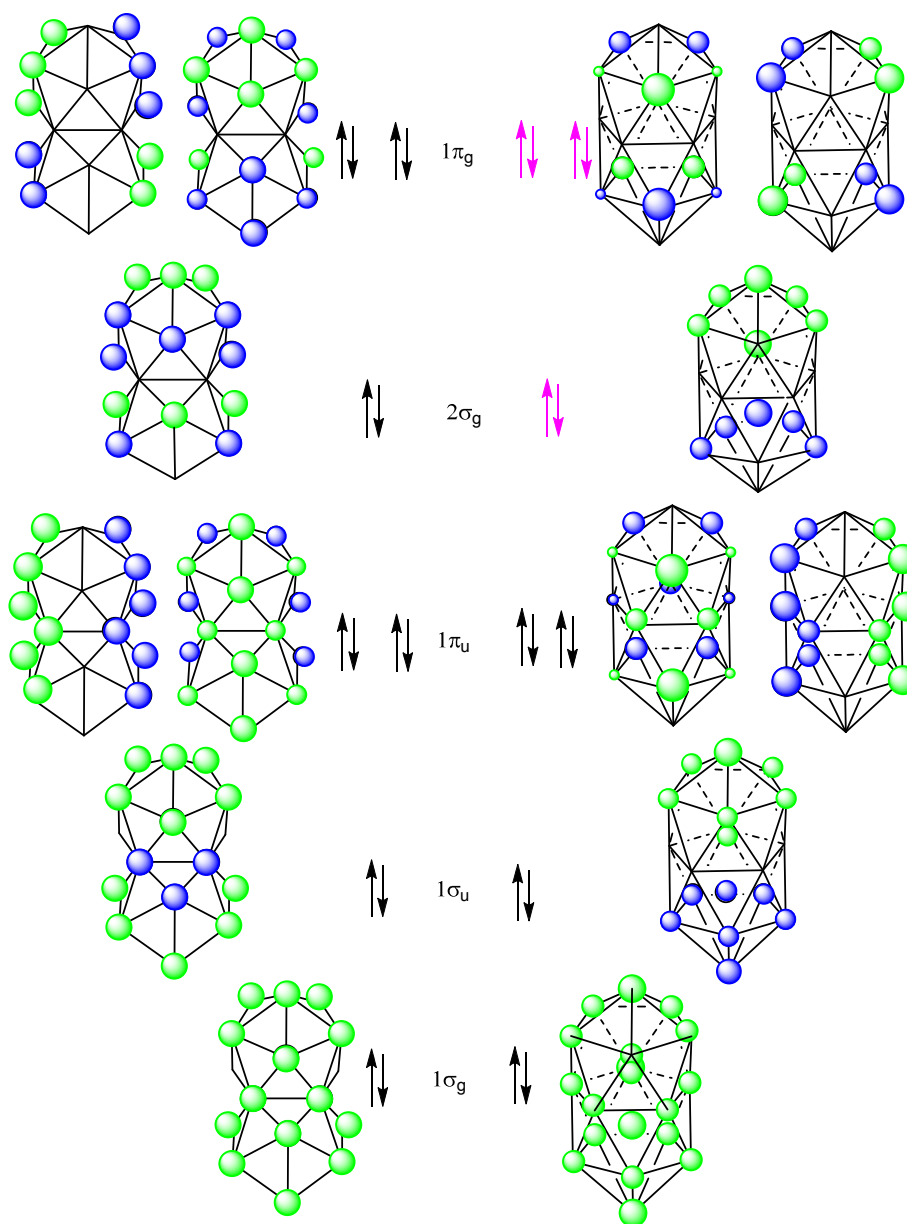


**Figure C.** Schematic illustration of the skeletal molecular orbitals of an icosahedron sharing a triangular face ( $\text{sec} = 14$ ) and two interpenetrated icosahedra sharing a pentagonal face and an interstitial atom ( $\text{sec} = 8$  for (V) (black arrows) and  $= 16$  for (VI) (black and magenta arrows)).

## References

1. R.E. Williams, *Inorg. Chem.*, 1971, **10**, 210-214.
2. K. Wade, *J. Chem. Soc. Chem. Commun.*, 1971, 792-7933.
3. D.M.P. Mingos, *Nature Phys. Sci.*, 1972, **236**, 99-102.
4. R.W. Rudolph and W.R. Pretzer, *Inorg. Chem.*, 1972, **11**, 1974-1978.
5. Thomas KM, Mason R, Mingos DMP, *J. Amer. Chem. Soc.*, 1973, **95**, 802-804.
6. D.M.P. Mingos and M.I. Forsyth, *J. C. S. Dalton Trans.*, 1977, 610-616.
7. M. Elian, M.M.L. Chen, D.M.P. Mingos and R. Hoffmann, 1976, **15**, 1148-1155.
8. D.M.P. Mingos, *J. Chem. Soc. Dalton Trans.*, 1974 133-138.
9. D.M.P. Mingos, *J. Chem. Soc. Dalton Trans.*, 1977, 602-610.
10. D.M.P. Mingos, M.I. Forsyth and A.J. Welch, *J. Chem. Soc. Chem. Commun.*, 1977, 605-607.
11. D.M.P. Mingos, D.N. Cox and R. Hoffmann, *J.C.S. Dalton Trans.*, 1981, 1788-1797.
12. D.M.P. Mingos and M.J. Calhorda, *J. Organomet. Chem.*, 1982, **229**, 229-245.
13. D.M.P. Mingos and D.G. Evans, *J. Organomet. Chem.*, 1982, **232**, 179-191; 1982, **240**, 321-327..
14. K. Wade, *Adv. Inorg. Radiochem.*, 1976, **18**, 1-66.
15. D.M.P. Mingos, *J. Chem. Soc. Dalton Trans.*, 1976, 1163-1169.
16. P.J. Dyson, and D.M.P. Mingos, in *Gold Progress in Chemistry, Biochemistry and Technology*, Ed H. Schmidbaur (1999), John Wiley and Sons, Chichester UK 512-513
17. K.P. Hall and D.M.P. Mingos, *Prog. Inorg. Chem.*, 1984, **32**, 237-325.
18. D.M.P. Mingos and M.J. Watson, *Adv. Inorg. Radiochem.*, 1992, **39**, 327-399.
19. D.M.P. Mingos, *Phil. Trans. Roy. Soc. (London)*, 1982, **308**, 75-83.
20. C.F. Briant, B.R.C. Theobald, J.W. White, L.K. Bell, D.M.P. Mingos and A.J. Welch, *J. Chem. Soc. Chem. Commun.*, 1981, 201-202.
21. H. Schmidbaur, A. Grohmann and M.E. Olmos, in *Gold Progress in Chemistry, Biochemistry and Technology*, Ed H. Schmidbaur, John Wiley and Sons, Chichester UK, 1999, 648-731.
22. O. Steigelmann, P. Bissinger and H. Schmidbaur, *Angew. Chem. Int. Ed.*, 1990, **27**, 1544; **29**, 1399-1400; 1991, **30**, 1488-1490.
23. L.H. Pignolet and D.A. Krogstad, in *Gold Progress in Chemistry, Biochemistry and Technology*, Ed H. Schmidbaur, John Wiley and Sons, Chichester UK, 1999, 430-465.
24. D.M.P. Mingos in *Chemistry of the Copper and Zinc Triads*: Royal Society of Chemistry Special Publication, 1993. **131**, 189-197.
25. D.M.P. Mingos, *J. C. S. Dalton Trans.*, 1996, 561-566.
26. M. Brust, M. Walker, D. Bethell, D.J. Schiffrin and R. Whyman, *J. Chem. Soc. Chem Commun.* 1994, 801-802.
27. C.J. Kiely, J. Fink, M. Brust, M. Walker, D. Bethell and G.J. Schiffrin, *Nature*, 1998, **396**, 444-446.
28. M-C. Daniel and D. Astruc, *Chem. Rev.* 2004, **104**, 93-346.
29. M. Walter, J. Akola, O. Lopez-Acevedo, P.D. Jadinsky, G. Calero, C.J. Ackerson, R.L. Whetten, H. Grönbeck, H. Häkkinen, *Proc Acad Natl Sci USA*, 2008. **105**, 9157-9162.
30. M.W. Heaven, A. Dass, P.S. White, K.M. Holt and R.W. Murray, *J. Am. Chem. Soc.*, 2008, **130**, 3754-3756.
31. H. Häkkinen, M. Walter and H. Grönbeck, *J Phys Chem B*, 2006 **110**, 9927-9931.
32. Häkkinen H, R.N. Barnett and U. Landman, *Phys. Rev. Lett.*, 1999, **82**, 3264; *Science*, 1999, **318**, 430-4333.
33. H. Häkkinen, *Chem. Soc. Rev.*, 2008, **37**, 1847-1859.
34. K Salorinne K, T Lahtinen T, J Koivisto J, Kalenius, E Nissinen, Maija PM, H. Häkkinen, *Anal Chem.* 2013, **85**, 3489-3492.

35. H. Häkkinen in Metal Nanoparticles and Nanoalloys Ed R.L. Johnston and J.P. Wilcoxon, in *Frontiers of Nanoscience*, Series Editor R.E. Palmer, Elsevier, Amsterdam, Holland, 2012, **3**, 129-154
36. H. Häkkinen in Theoretical Studies on Gold Nano-Particles in Various Environments: When the Size Matters, Gold Particles in Physics, Biology and Chemistry, Ed. C. Louis and O. Pluchery, 2012, 233-272.
37. H. Häkkinen, *Nature Chem.*, 2012, **4**, 443-455.
38. Y. Peng and X.C. Zeng, *Nanoscience*, 2012, **4**, 4054-4072.
39. D.M.P. Mingos, *Struct. Bond.*, 2014, **161**, 1-48.
40. W.D. Knight, K. Clemenger, De Heer, WA, Saunders WA, Winston A, Chou MY, and M.L. Cohen, *Phys. Rev. Lett.*, 1984, **52**, 2141-2143.
41. W.D. Knight, K. Clemenger, De Heer, WA, Saunders WA, Winston, *Solid State Commun.*, 1985, **53**, 445-446.
42. K. Clemenger, *Phys. Rev. B, Condens. Matt.*, 1985, **32**, 1359-1362.
43. D.J. Wales, D.M.P. Mingos, *Inorg. Chem.*, 1989, **28**, 2748-2754.
44. Z. Lin, R.P.F. Kanters and D.M.P. Mingos, *Inorg. Chem.* 1991, **30**, 91-5; D.M.P. Mingos, Z. Lin and T. Slee, *Chem. Rev.*, 1990, **90**, 383-402; *Chem. Phys.*, 1990, **142**, 321-334.
44. D.M.P. Mingos and R.L. Johnston, *Struct. Bond.* 1987, **68**, 1-82.
45. D.M.P. Mingos and R.L. Johnston, *J. Chem. Soc. Dalton Trans.*, 1987, 647-656 and 1445-1456.
46. R.L. Johnston, *Atomic and Molecular Clusters*, Taylor and Francis, New York, NY, USA, 2002.
47. D.M.P. Mingos, *J. Chem. Soc. Chem. Commun.*, 1985, 1352-1354.
48. A.J. Stone, *Inorg. Chem.*, 1981, **20**, 563-571.
49. A.J. Stone, *Polyhedron*, 1983, **3**, 1299-1306.
50. Z. Lin, R.P.F. R.P.F. Kanters and D.M.P. Mingos, *Inorg. Chem.*, 1991, **30**, 91-95.
51. N.T. Tran, M. Kawano, L.F. Dahl, *J. C. S. Dalton Trans.*, 2001, 2731-2748.
52. N.T. Tran, D.R. Powell, and L.F. Dahl, *Angew. Chem. Intern. Ed.*, 2000, **39**, 4121-4125.
53. N.T. Tran, M. Kawano and L.F. Dahl, *Angew. Chem, Intern. Ed.* 2003, **42**, 3533-3537.
54. A. Bernardi, C. Femoni, M.C. Iapalucci, G. Longoni, F. Ranuzzi, S. Zacchini, P. Zanella, and S. Fedi, *Chemistry*, 2008, **14**, 1924-1934.
55. G. Longoni, C. Femoni, M.C. Iapalucci and P. Zanella in *Metal Clusters in Chemistry*, (Eds.: P. Braunstein, L.A. Oro, P.R. Raithby), Wiley-VCH, Weinheim, 1999, 1137 – 1158; b) G. Longoni and M.C. Iapalucci in *Clusters and Colloids* (Ed.: G. Schmid), Wiley-VCH, Weinheim, 1994, 91 – 177.
56. B.K. Teo, *Polyhedron*, 1988, **8**, 2317-2320.
57. B.K. Teo, Z. Shi and H. Zhang, *J. Am. Chem. Soc.* 1992, **114**, 2473-2745.
58. Herzberg G, *Molecular Structure and Molecular Spectra*, Van Nostrand, New York, USA, 1967, III, 276-419.
59. R.S. Mulliken, *Phys. Rev.*, 1932, **40**, 55-62, 1932, **41**, 49-71; 1932, **41**, 751-758.
60. J.R. Lowe, *Quantum Chemistry*, Academic Press, New York, 1978, 167-192.
61. Dass, T. Li, K. Nobosada, C. Zeng, N.L. Rosi, and R. Jin, *J. Am. Chem. Soc.*, 2013, **135**, 18264-18267.
62. D. Crasto, G. Barcaro, M. Stener, L. Sementa, A. Fortunelli and A. Dass, *J. Am. Chem. Soc.*, 2014, **136**, 14933-14940.
63. S. Crosta, S. Malola, G. Brosofsky, A. Dass, H. Häkkinen, *J. Am. Chem. Soc.*, 2014, **136**, 5000-5002.
64. D.M.P. Mingos, unpublished work and see reference 45.
65. K. Konishi, *Struct. Bond.*, 2014, **161**, 49-86.

66. Y. Shichibu, K. Konishi, *Inorg. Chem.*, 2013, **52**, 6570-6575.
67. Y. Shichibu, Y. Kamei, K. Konishi, *J. C. S. Chem. Commun.*, 2012, **48**, 7559-7561
68. Y. Kamei, Y. Shichibu, K. Konishi, *Angew. Chem. Int. Ed.*, 2011, **50**, 7442-7445.
69. C. Zeng, H. Qian, T. Li, G. Li, N.L. Rosi, B. Yoon, R.N. Barnett, R.L. Whetten, U. Landman and R. Jin, *Angew. Chem. Int. Ed.*, 2012, **51**, 13114-13118.
70. X.K. Wan, Z.W. Win, and Q.M. Wang, 2012, **134**, 14750-2.
71. B. Gutrath, I. Oppel, O. Presly, I. Beljakov, V. Meded, W. Wenzel, and U. Simon, *Angew. Chem. Int. Ed.*, 2013, **52**, 3529-3532.
72. C. Zeng, C. Liu, Y. Chen, N.L. Rosi and R. Jin, *J. Am. Chem. Soc.* 2014, **136**, 11922-11925.
73. D.M.P. Mingos, Editor, *Gold, Clusters and Nano-Particles I, Struct. Bond.*, Springer, Heidelberg, 2014, **161**, 1-282,
74. D.M.P. Mingos, Editor, *Gold, Clusters and Nano-Particles II, Struct. Bond.*, Springer, Heidelberg, 2014, **162**, 1-223.